*Supplement of*

# Strong Primary contribution to Brown Carbon light absorption in Tibet and urban areas: insights based on in situ measurement

**Wenhui Zhao et al.**

Correspondence to: Weiwei Hu (E-mail：weiweihu@gig.ac.cn)； Shan Huang (Email: shanhuang_eci@jnu.edu.cn)

## Supplementary Information Contents:

# Text S1. Positive matrix factorization (PMF) analysis

Positive matrix factorization (PMF) was performed on the high-resolution mass spectra of organic aerosol (OA) of the SP-AMS at the YBJ site. The solutions of factor 1–8 with fpeak varied from -1 to 1 were run. The $Q/Q_{exp}$, scaled residuals, comparison between mass spectra of individual factors, diurnal variation of each factor, and comparison of the temporal evolution of every factor with corresponding external tracers were used to identify the best correlation for determining the optimum number of factors. The detailed steps were listed in a previous study (Zhang et al., 2011). As shown in Fig. S2, 5–factors solution (fpeak = 0) is the best solution, including biomass burning OA (BBOA), hydrocarbon-like OA (HOA), BBOA mixed with cooking-related OA (COA) (biofuel–OA), less-oxidized oxygenated OA (LO-OOA), and more-oxidized oxygenated OA (MO-OOA) (Fig. S4). The OA source apportionment at the YBJ site will be reported by Liang et al. (2025) *(in preparation)*. At the GIG site, unconstrained PMF (factor 1–8 with fpeak varied from -1 to 1) was also first performed on the OA measured by the ToF–ACSM (Fig. S2). However, we didn't find the best solution due to the ambiguous factor3 in the 5 factor-solution as shown in Fig. S2 and S3. We furtherly constrained BBOA applying the standard BBOA mass spectra (Hu et al., 2016; Hu et al., 2013) with a wide range of a value (e.g., a value = 0–1) based on Multilinear Engine 2 (ME-2; SoFi 6.8) (Canonaco et al., 2013). Finally, we selected an optimum solution of 5 factors in ME-2 with a value=0 (Fig. S4), including COA, BBOA, HOA, LO-OOA, and MO-OOA.

**Biomass burning OA (BBOA) and Biofuel–OA**

The BBOA component was identified at the YBJ site with an obvious peak at m/z 60 ($C_2H_4O_2^+$) and 73 ($C_3H_5O_2^+$) signals in the MS (Fig. S4), which are usually considered as a recognized tracer emitted from biomass burning (Alfarra et al., 2007). Different from the BBOA factor in other cities in eastern China, which is mainly from burning of residual straw or wood for heating, the BBOA in Tibet was mainly from wormwood, cypress branches, highland barley, yak butter, zanba, and so on (Cui et al., 2018; Zhang et al., 2020b). The diurnal variation in BBOA therefore (Fig. S4) showed a unique diurnal pattern with two peaks in the morning (~ 8:00) and evening (20:00–21:00). This pattern was mainly related to the lifecycle of residents in Tibet, who routinely perform "Weisang" activity during the morning and evening each day. The BBOA component identified at GIG site showed different diurnal variation with enhanced afternoon and nighttime peaks likely reflect regional transport of biomass burning emissions from agricultural activities in the Pearl River Delta region during summer (Cai et al., 2023; Wang et al., 2017).

The Biofuel-OA component at the YBJ site was characterized by the highest m/z 55 ($C_3H_3O^+$) signal and a higher ratio of m/z 55/57 compared with HOA (Zhang et al., 2011), as well as the m/z 73 ($C_3H_5O_2^+$) signal. The time series of biofuel-OA component showed a close correlation with emissions of tracking ions fragments $C_3H_3O^+$ (R=0.8) and $C_6H_{10}O^+$ (R=0.93) (Fig. S5), which were also highly correlated with the emissions of biomass burning fragments $C_2H_4O_2^+$ (R=0.93). These findings demonstrated that this factor was associated with emissions of biomass burning and cooking. In this study at YBJ site, the diurnal variation in COA showed three notable peaks corresponding to breakfast time (8:00), lunchtime (13:00), and dinner time (21:00) in Tibet, while

peaks occurred at 7:00, 12:00 and 19:00 for GIG site, which coincided with different schedules between urban Guangzhou and remote Tibet.

**Hydrocarbon-like OA (HOA)**

The HOA component identified at the YBJ site, sourced from traffic emissions and/or other fossil fuel burning activities, presented a high-resolution mass spectrum (Fig. S4) resembling that of former research (Zhang et al., 2011; Ulbrich et al., 2009; Hu et al., 2016; Xu et al., 2014). The hydrocarbon ion series of $C_xH_y^+$ dominated the MS of HOA; therein $C_3H_5^+$, $C_3H_7^+$, $C_4H_7^+$, $C_4H_9^+$, $C_5H_9^+$ and $C_5H_{11}^+$ (m/z = 41, 43, 55, 57, 69, 71) were the main constituents (Ng et al., 2011a; Zhang et al., 2005b; Xu et al., 2014; Zhang et al., 2019). The O/C ratio of HOA in this study was 0.11, suggesting its fresh property. The tight correlation between HOA versus BC and $C_4H_9^+$ (R = 0.53 and 0.92; Fig. S5a) also indicated that the source of HOA was from traffic emissions. In addition, two distinct peaks of HOA occurred in the morning (8:00-9:00) and evening (20:00-21:00) rush hours (Fig. S4). All these characteristics suggested a reasonable decomposition for HOA. At the GIG site, HOA displayed a bimodal distribution with a moderate morning peak at 07:00 and a stronger evening peak at 20:00 (Fig. S4), consistent with typical urban HOA diurnal patterns. The enhanced evening peak coincides with rush-hour traffic congestion, suggesting intensified vehicular emissions during these periods. Notably, the evening peak magnitude exceeds morning levels, potentially reflecting combined effects of meteorological conditions (e.g., reduced boundary layer height) and emission intensity.

**Oxygenated OA (OOA)**

The mass spectra of MO-OOA and LO-OOA at the YBJ site were characterized by high peaks at m/z 44 (mostly $CO_2^+$) and LO-OOA had a larger peak at m/z 43 (mostly $C_2H_3O^+$) as well (Crippa et al., 2013; Hu et al., 2016; Lanz et al., 2007; Sun et al., 2010; Zhang et al., 2005a). As a highly oxidizing species, MO-OOA is consistent with the time variation of sulfate (R=0.74; Fig. S5a). Among all OA factors, MO-OOA had the highest O/C (0.78) and the lowest H/C (1.40), indicating a high oxidation degree of this factor, while LO-OOA had the lower O/C (0.55). There is a good correlation between the LO-OOA factor time series and the characteristic ion fragments $C_2H_3O^+$ and $C_3H_3O^+$ with R of 0.95 and 0.75 (Fig. S5a), respectively. The diurnal variation of LO-OOA and MO-OOA was characterized by high values during the day and low values at night, with the fact that MO-OOA concentrations (6:00) increased approximately two hours later than LO-OOA (8:00) during the daytime, indicating different degrees of photochemical aging of local or regional aerosols under strong solar radiation. At the GIG site, the mass spectrum of the MO-OOA was similar to the MO-OOA of the YBJ site, with high peaks at m/z 44 and the diurnal pattern, demonstrating that MO-OOA was significantly influenced by aging processes, in particular photochemistry. The concentration of MO-OOA showed a better correlation with that of sulfate (R = 0.87) than with nitrate (R = 0.7) (Fig. S5b), which is likely attributed to similarly high oxidation degrees of both MO-OOA and sulfate. The LO-OOA component identified at the GIG site is also characterized by a high m/z 44 signal but lower than that of MO-OOA, indicating its relatively fresh Features.

## Text S2. Uncertainty analysis for the MLR method.

Before the MLR method was applied, the correlations between the BrC absorption coefficients at 370nm ($Abs_{BrC,370nm}$) and the mass loadings of OA factors were evaluated as shown in Fig. S9. Results show that BBOA and HOA concentrations were well correlated with $Abs_{BrC,370nm}$ (R = 0.77 and R = 0.64). A moderate correlation (R = 0.31) was also found between $Abs_{BrC,370nm}$ and the LO-OOA mass concentration. The correlation for MO-OOA was near zero, indicating that aging may have reduced the absorption capacity. In addition, the correlation coefficient of each PMF factor was also performed for each campaign. At the YBJ site, it shows that the BBOA factor correlated strongly with the biofuel-OA factor (R = 0.89; Fig. S5a), which caused multicollinearity issues. To solve this issue, we set four different cases via combining or removing the latent collinearity factors to test the sensitivity of the MLR method, including considering all five individual factors (case 1), removing biofuel-OA (case 2), combining BBOA and biofuel-OA (case 3), and removing BBOA (case 4), as shown in Table S2.

At the GIG site, due to the strong similarity among time series of each factor (while different mass spectral profiles as shown in Fig. S4), the factors, except HOA, showed varying degrees of strong correlation with each other, as shown in Fig. S5b. And all OA factors were well or moderately correlated with $Abs_{BrC,370nm}$ (Fig. S9). Based on these problems, we set up three scenarios to test the sensitivity of the MLR method, including considering all five individual factors (case 1) and combining all collinearity factors except HOA (case 2). In addition, we also consider the hypothesis that only BBOA and HOA are absorptive (case 3).

To get the best final solution, we calculated the total uncertainty of the MLR regression coefficients (i.e., MAC) for each case using Monte Carlo. For the Monte Carlo calculation input, the uncertainty of the PMF factor mass concentration needs to be evaluated. A bootstrap analysis (100 iterations; (Ulbrich et al., 2009) was applied, which shows a 9–36 % uncertainty for the PMF factors at the YBJ site and 3 – 9 % at the GIG site, as shown in Table S3. The uncertainty for the coefficient of BrC at 370 nm calculated using $AAE_{BC} = 1$ was estimated to be 43 % for the YBJ site and 36 % for the GIG site based on the lower (0.8) and upper limit of (1.2) previously reported $AAE_{BC}$ range. The total uncertainties of each coefficient for each PMF factor were then calculated by Monte Carlo with 10,000 simulations.

Monte Carlo results show a high total uncertainty (Table S4) of the factors when we don't deal with collinearity at all (i.e., case 1) at both sites, indicating that the collinearity problem among the factors does increase the uncertainty of the MLR regression coefficients (i.e., MAC).
Combining or removing collinearity factors (i.e., case 2–4 for the YBJ site or case 2–3 for the GIG site) can effectively reduce the uncertainty.

Considering that biomass burning is widely reported as an important source of BrC light absorption and regarded as a warming agent affecting global climate (Wang et al., 2025), we consider all biomass burning related contributing sources when run the MLR model in the case of eliminating the collinearity problemin in this study. As previously reported in the literature (Kasthuriarachchi et al., 2020a; Qin et al., 2018), the MAC of COA is nearly zero. Thus, the

absorption of light by COA was not considered in this study. For the YBJ site, we finally combined the BBOA factor and the biofuel-OA factor as BBOA (case3). The final results show an uncertainty of BBOA (26.4 %), HOA (20.8 %), LO–OOA (56.3 %), and MO-OOA (57.9%), as shown in Table S4. For the GIG site, we consider only including BBOA and HOA as input variables (case 3) for MLR at the GIG site. And the final results show an uncertainty of HOA (5.8 %), BBOA (6.8 %), and intercept (21.6 %).

We also evaluate the lower and upper limits of the proportion of different sources contributing to the BrC light absorption under all case scenarios. At the YBJ site, the lower limit of MAC is 1.11, 2.04. 0.07 and 0.07 $m^2 g^{-1}$ for BBOA, HOA, LO–OOA, and MO–OOA, while the upper limit of MAC is 2.54, 2.36, 0.23, and 0.29 $m^2 g^{-1}$ for BBOA, HOA, LO–OOA, and MO–OOA. At the GIG site, the lower limit of MAC is 1.91 and 2.57 $m^2 g^{-1}$ for BBOA and HOA, while the upper limit is 2.63 and 0.16 $m^2 g^{-1}$ for HOA and BBOA+LO–OOA+MO–OOA. As shown in Fig. S8, at the YBJ site, BBOA was the significant contributor to BrC light absorption (46 %–54 %), followed by HOA (26 %–43 %) and SOA (11 %–20 %). At the GIG site, HOA was the significant contributor to BrC light absorption (50–54 %), followed by BBOA (36 %) and SOA (0–33 %). Regardless of the case, BBOA is still the dominant absorption contributor at the YBJ site, while HOA is the dominant absorption contributor at the GIG site, as well as the dominant contribution of POA to BrC light absorption in both sites, indicating the robust conclusion in this study.

**Table S1.** The summary of BrC light absorption coefficients and the contributions at 370 nm, as well as the OA mass concentration and primary OA fraction, are based on the literature results. The results were categorized according to the locations of their observation sites (Arctic region, Qinghai–Tibet Plateau (QTP region), Southern China, and Northern China).

| Sites | $Fraction_{BrC}$ (%) | $Abs_{BrC}$ (M $m^{-1}$) | OA (μg $m^{-3}$) | $Fraction_{POA}$ (%) | References |
|---|---|---|---|---|---|
| **Arctic region** | | | | | |
| circum–Arctic | | 0.1 | | | (Yue et al., 2022) |
| Alert | | 0.04 | | | (Yue et al., 2019) |
| Utqiagvik, Alaska | | 0.2 | | | (Barrett and Sheesley, 2017) |
| **QTP region** | | | | | |
| Lhasa (Autumn) | 8 | 4.2 | | | (Zhu et al., 2017) |
| Beiluhe (Summer) | 12.0 | 1.6 | | | (Zhu et al., 2021) |
| Beiluhe (Autumn) | 15.2 | 2.4 | | | (Zhu et al., 2021) |
| YBJ site (Summer; **This study**) | 15.4 | 0.2 | 0.7 | 34 | |
| Beiluhe (Spring) | 16.2 | 1.9 | | | (Zhu et al., 2021) |
| Beiluhe (1 year) | 18.0 | 2.0 | | | (Zhu et al., 2021) |
| NamCo (Spring+Summer) | 21.3 | 0.7 | | | (Zhang et al., 2021b) |
| WLG(Summer) | 22.4 | 0.6 | | | (Zhang et al., 2021b) |
| Beiluhe (winter) | 25.9 | 2.1 | | | (Zhu et al., 2021) |
| Ngari (Autumn) | 27.4 | 7.6 | | | (Zhu et al., 2021) |
| Ngari (Summer) | 31.4 | 5.9 | | | (Zhu et al., 2021) |
| Lulang (Autumn) | 32.0 | 4.8 | | | (Zhu et al., 2017) |
| QOMS (Spring) | 33.1 | 4.4 | 2.4 | 86 | (Zhang et al., 2021b) |
| Qinghai Lake (Summer) | 33.9 | 4.1 | | | (Zhu et al., 2021) |
| Ngari (one year) | 35.0 | 7.3 | | | (Zhu et al., 2021) |
| Ngari (Spring) | 36.7 | 6.1 | | | (Zhu et al., 2021) |
| Gaomeigu (Spring) | 37.0 | 12.3 | | | (Tian et al., 2023) |
| Qinghai Lake (Spring) | 38.6 | 9.3 | | | (Zhu et al., 2021) |
| Ngari (winter) | 40.7 | 10.7 | | | (Zhu et al., 2021) |
| Qinghai Lake (winter) | 43.0 | 9.6 | | | (Zhu et al., 2021) |
| Qinghai Lake (1 year) | 44.0 | 9.1 | | | (Zhu et al., 2021) |

| | | | | | |
|---|---|---|---|---|---|
| Qinghai Lake (Autumn) | 54.4 | 14.9 | | | (Zhu et al., 2021) |
| **Southern China** | | | | | |
| Hong Kong (Winter) | 11.0 | 6.3 | | | (Zhang et al., 2020a) |
| Nanjing (Summer) | 14.4 | 26.5 | | | (Bao et al., 2022) |
| Nanjing (Spring) | 16.1 | 29.7 | | | (Bao et al., 2022) |
| Nanjing (3 years) | 16.7 | 6.3 | | | (Wang et al., 2018) |
| Nanjing (Autumn) | 17.0 | 37.3 | | | (Bao et al., 2022) |
| Nanjing (Winter) | 19.6 | 51 | | | (Bao et al., 2022) |
| GIG site (Summer; **This study**) | 21.0 | 2.9 | 6.9 | 29 | |
| Guangzhou, Panyu (Winter) | 23.6 | 13.7 | 20 | 40 | (Qin et al., 2018) |
| Wuhan (Winter) | 28.7 | | | | (Zhang et al., 2021a) |
| **Northern China** | | | | | |
| Xian (Winter, Normal) | 29.0 | 49.4 | 43.3 | 49 | (Zhang et al., 2022) |
| Beijing (Winter 2020) | 36.0 | 24 | 11.25 | 56.3 | (Sun et al., 2021) |
| Shanghai (Winter) | 37.6 | | | | (Zhang et al., 2021a) |
| Gucheng (Winter) | 38.0 | 66.5 | 21.33 | 51.2 | (Sun et al., 2021) |
| Harbin (Winter) | 40.6 | | | | (Zhang et al., 2021a) |
| Beijing (Winter 2016) | 46.0 | | | 77 | (Xie et al., 2019) |
| Xian (Winter, Lockdown) | 49.0 | 47.7 | 29.4 | 44 | (Zhang et al., 2022) |
| Xianghe (Winter) | 58.0 | 61.8 | | | (Wang et al., 2019) |

**Table S2.** Regression coefficients (MAC) of the multiple linear regression (MLR) at 370,470, 520, 590, and 660 nm at the YBJ site and GIG site.

## YBJ site

| | | Wavelength (nm) | | | | |
|---|---|---|---|---|---|---|
| | | 370nm | 470nm | 520nm | 590nm | 660nm |
| **Case1** | BBOA | 2.54±0.53 | 0.66±0.25 | 0.25±0.18 | 0.11±0.11 | 0±0.13 |
| | HOA | 2.36±0.31 | 1.16±0.14 | 0.20±0.1 | 0.16±0.06 | 0±0.08 |
| | LO–OOA | 0.07±0.08 | 0.13±0.04 | 0.06±0.03 | 0.04±0.02 | 0±0.02 |
| | MO–OOA | 0.29±0.19 | 0.20±0.09 | 0±0.06 | 0.02±0.04 | 0±0.05 |
| | biofuel–OA | 0±0.42 | 0.22±0.20 | 0±0.14 | 0.10±0.09 | 0±0.1 |
| | intercept | 0±0.02 | 0.02±0.01 | 0.04±0.01 | 0.02±0 | 0.03±0 |
| **Case2** | biofuel–OA | 1.80±0.19 | 0.70±0.09 | 0.18±0.06 | 0.18±0.04 | 0±0.04 |
| | HOA | 2.04±0.32 | 1.08±0.14 | 0.17±0.1 | 0.15±0.06 | 0±0.07 |
| | LO–OOA | 0.23±0.08 | 0.17±0.03 | 0.08±0.02 | 0.05±0.01 | 0.01±0.02 |
| | MO–OOA | 0.07±0.19 | 0.15±0.09 | 0±0.06 | 0.01±0.04 | 0±0.04 |
| | intercept | 0±0.02 | 0.02±0.01 | 0.04±0.01 | 0.02±0 | 0.03±0 |
| **Case3** | BBOA+ biofuel–OA | 1.11±0.11 | 0.42±0.05 | 0.11±0.03 | 0.11±0.02 | 0±0.03 |
| | HOA | 2.08±0.30 | 1.11±0.14 | 0.18±0.1 | 0.16±0.06 | 0±0.07 |
| | LO–OOA | 0.15±0.08 | 0.14±0.03 | 0.07±0.02 | 0.04±0.02 | 0.01±0.02 |
| | MO–OOA | 0.18±0.18 | 0.19±0.08 | 0±0.06 | 0.02±0.04 | 0±0.04 |
| | intercept | 0±0.02 | 0.02±0.01 | 0.04±0.01 | 0.02±0 | 0.03±0 |
| **Case4** | BBOA | 2.54±0.23 | 0.92±0.11 | 0.25±0.08 | 0.23±0.05 | 0±0.06 |
| | HOA | 2.36±0.28 | 1.24±0.13 | 0.20±0.09 | 0.20±0.06 | 0±0.07 |
| | LO–OOA | 0.07±0.08 | 0.12±0.04 | 0.06±0.03 | 0.04±0.02 | 0±0.02 |
| | MO–OOA | 0.29±0.18 | 0.22±0.09 | 0±0.06 | 0.03±0.04 | 0±0.04 |
| | intercept | 0±0.02 | 0.02±0.01 | 0.04±0.01 | 0.02±0 | 0.03±0 |

## GIG site

| | | Wavelength (nm) | | | | |
|---|---|---|---|---|---|---|
| | | 370nm | 470nm | 520nm | 590nm | 660nm |
| **Case1** | COA | 0.78±0.39 | 0.17±0.19 | 0.05±0.11 | 0.04±0.08 | 0±0.04 |
| | BBOA | 0±3.23 | 0±1.51 | 0±0.87 | 0±0.63 | 0±0.31 |
| | HOA | 1.67±0.48 | 1.32±0.24 | 0.72±0.14 | 0.40±0.1 | 0.17±0.05 |
| | LO–OOA | 0±0.35 | 0±0.17 | 0±0.09 | 0±0.07 | 0±0.03 |
| | MO–OOA | 0.19±0.34 | 0.11±0.16 | 0.04±0.07 | 0.05±0.07 | 0.03±0.03 |
| | intercept | 0.57±0.19 | 0.22±0.09 | 0.43±0.05 | 0.17±0.04 | 0.11±0.02 |
| **Case2** | HOA | 2.93±0.27 | 1.57±0.12 | 0.79±0.07 | 0.45±0.05 | 0.16±0.03 |
| | BBOA+LO–OOA+MO–OOA | 0.16±0.02 | 0.08±0.01 | 0.03±0 | 0.03±0 | 0.02±0 |
| | intercept | 0.34±0.17 | 0.17±0.08 | 0.41±0.05 | 0.16±0.03 | 0.11±0.02 |
| **Case3** | HOA | 2.57±0.28 | 1.40±0.13 | 0.72±0.07 | 0.38±0.06 | 0.13±0.03 |
| | BBOA | 1.91±0.21 | 0.90±0.10 | 0.35±0.06 | 0.40±0.04 | 0.20±0.02 |
| | intercept | 0.37±0.17 | 0.18±0.08 | 0.42±0.04 | 0.17±0.03 | 0.11±0.02 |

**Table S3.** Quantitative assessment of the uncertainty of the PMF factors was made by bootstrapping analysis with 100 iterations.

| YBJ site | Uncertainty | GIG site | Uncertainty |
|---|---|---|---|
| BBOA | 23% | BBOA | 5% |
| HOA | 36% | HOA | 4% |
| biofuel–OA | 23% | COA | 4% |
| LO–OOA | 9% | MO–OOA | 3% |
| MO–OOA | 15% | LO–OOA | 5% |
| BBOA+ biofuel–OA | 33% | BBOA+MO–OOA+LO–OOA | 8% |
| $Abs_{BrC,370nm}$ | 43% | $Abs_{BrC,370nm}$ | 36% |

**Table S4.** The uncertainty of multiple linear regression (MLR) at 370 nm using Monte Carlo simulations at the YBJ site and GIG site.

## YBJ site

| CASE | | Mean | Standard deviation | Uncertainty (%) (100*std/mean) |
|---|---|---|---|---|
| Case1 | BBOA | 2.06 | 0.81 | 39.3 |
| | HOA | 2.07 | 0.39 | 19.0 |
| | LO–OOA | 0.10 | 0.09 | 88.1 |
| | MO–OOA | 0.27 | 0.11 | 42.7 |
| | biofuel–OA | 0.43 | 0.49 | 114.3 |
| | intercept | 0 | 0 | |
| Case2 | biofuel–OA | 1.78 | 0.43 | 24.2 |
| | HOA | 1.91 | 0.42 | 22.0 |
| | LO–OOA | 0.22 | 0.07 | 33.2 |
| | MO–OOA | 0.11 | 0.09 | 83.5 |
| | intercept | 0 | 0 | |
| Case3 | BBOA+ biofuel–OA | 1.06 | 0.28 | 26.4 |
| | HOA | 2.02 | 0.42 | 20.8 |
| | LO–OOA | 0.16 | 0.09 | 56.2 |
| | MO–OOA | 0.19 | 0.11 | 57.9 |
| | intercept | 0 | 0 | |
| Case4 | BBOA | 2.55 | 0.60 | 23.4 |
| | HOA | 2.22 | 0.37 | 16.7 |
| | LO–OOA | 0.09 | 0.09 | 97.2 |
| | MO–OOA | 0.29 | 0.11 | 37.6 |
| | intercept | 0 | 0 | |

## GIG site

| CASE | | Mean | Standard deviation | Uncertainty (%) (100*std/mean) |
|---|---|---|---|---|
| Case1 | COA | 0.74 | 0.14 | 19.5 |
| | BBOA | 0.23 | 0.49 | 216.4 |
| | MO–OOA | 0.16 | 0.06 | 37.5 |
| | HOA | 1.72 | 0.26 | 15.1 |
| | LO–OOA | 0.00 | 0.02 | 552.3 |
| | intercept | 0.57 | 0.08 | 14.8 |
| Case2 | BBOA+MO–OOA+LO–OOA | 0.16 | 0.01 | 6.2 |
| | HOA | 2.98 | 0.18 | 6.0 |
| | intercept | 0.35 | 0.08 | 23.5 |
| Case3 | BBOA | 1.87 | 0.11 | 5.8 |
| | HOA | 2.62 | 0.18 | 6.8 |
| | intercept | 0.38 | 0.08 | 21.6 |

**Table S5.** The summary of campaign–averaged light absorption coefficients (M $m^{-1}$) of total aerosols, BC, and BrC, as well as the BrC contribution to the total absorption of particles ($f_{BrC}$, %).

| Average ± SD | | 370nm | 470nm | 520nm | 590nm | 660nm | 880nm |
|---|---|---|---|---|---|---|---|
| YBJ | Total | 1.59±1.59 | 1.19±1.24 | 1.01± 1.05 | 0.88± 0.92 | 0.76±0.80 | 0.58±0.60 |
| | BC | 1.34±1.46 | 1.06±1.15 | 0.96±1.04 | 0.84±0.92 | 0.75±0.82 | 0.58±0.60 |
| | BrC | 0.22±0.32 | 0.13±0.17 | 0.05±0.08 | 0.03± 0.05 | 0.02±0.03 | 0 |
| | $f_{BrC}$ | 15.4±14.0 | 13.0±13.2 | 8.5±13.4 | 6.4±11.5 | 5.2±11.8 | 0 |
| GIG | Total | 13.2±7.0 | 9.5±5.1 | 8.1±4.4 | 7.1±3.7 | 6.1±3.3 | 4.4±2.4 |
| | BC | 10.5±5.6 | 8.3±4.4 | 7.5±4.0 | 6.6±3.5 | 5.9±3.1 | 4.4±2.4 |
| | BrC | 2.9±2.0 | 1.5±0.9 | 1.1±0.5 | 0.6± 0.4 | 0.3± 0.2 | 0 |
| | $f_{BrC}$ | 21.0±7.8 | 14.9±6.2 | 12.5±7.8 | 8.5±4.3 | 5.1±3.4 | 0 |

**Table S6.** The summary of OA factors contributing to BrC absorption at 370 nm using the PMF–MLR method. The asterisks (*) represent the absorption contributions of soluble BrC from different sources at 365nm. The sources include POA (primary OA) (BBOA (biomass burning OA), HOA (hydrocarbon–like OA), CCOA (coal combustion OA), COA (cooking–related OA), NOA (nitrogen-containing OA); If other types of BrC primary sources exist in the literature, they are unified as POA and SOA (secondary OA).

| Sites | BBOA | HOA | CCOA | COA | NOA | *POA | *SOA* | Unidentified | References |
|---|---|---|---|---|---|---|---|---|---|
| **China** | | | | | | | | | |
| Gucheng (winter) | (16%) | (10%) | (42%) | | | | (52%) | | (Sun et al., 2021) |
| Beijing (winter 2016) | (17%) | | (48%) | (3%) | | | (32%) | | (Xie et al., 2019) |
| Beijing (winter 2020) | | | (56%) | (7%) | | | (37%) | | (Sun et al., 2021) |
| Xianghe (winter) | (49%) | (4%) | (28%) | | | | (19%) | | (Wang et al., 2019) |
| $Xian_{lockdown}$ (winter) | (20%) | (11%) | (28%) | | | | (40%) | (1%) | (Zhang et al., 2022) |
| $Xian_{normal}$ (winter) | (17%) | (20%) | (45%) | | | | LO–OOA (12%) | (6%) | |
| Guangzhou(summer; **This study**) | (36%) | (51%) | | | | | | (13%) | |
| Guangzhou (Winter 2014) | (25%) | (23%) | | | | | LV–OOA (52%) | | (Qin et al., 2018) |
| **QTP region** | | | | | | | | | |
| Gaomeigu (Spring) | (51%) | | | | | | po–OOA (49%) | | (Tian et al., 2023) |
| QOMS (Spring) | (64%) | | | | (20%) | | MO–OOA (16%) | | (Zhang et al., 2021b) |
| YBJ (Summer; **This study**) | (40%) | (38%) | | | | | (22%) | | |
| **Other countries** | | | | | | | | | |
| Paris (winter) | (74%) | (8%) | | | | | OOA (18%) | | (Zhang et al., 2020c) |
| Delhi (winter) | (48%) | (10%) | | | | | SV–OOA (26%) | (16%) | (Singh et al., 2021) |
| Athens (winter) | (33%) | (13%) | | (13%) | | | (41%) | | (Kaskaoutis et al., 2021) |
| Singapore (winter) | | (83%) | | (2%) | | | LO–OOA (15%) | | (Kasthuriarachchi et al., 2020) |
| Manaus (Summer+Autumn) | (57%) | (22%) | | | | | (17%) | (4%) | (De Sá et al., 2019) |
| Mexico (winter) | (14%) | (54%) | | | | | (24%) | | |
| Mexico (Spring) | (55%) | (40%) | | | | | (0.2%) | (4.8%) | (Retama et al., 2022) |
| Mexico (Summer) | (6%) | (49%) | | | | | (5%) | (40%) | |
| Mexico (Winter to summer) | (43%) | (46%) | | | | | (6%) | (5%) | |
| ***Soluble BrC a 365nm** | | | | | | | | | |
| *Central Alabama (Summer) | (85%) | | | | | | LO–OOA (10%) | (3%) | (Washenfelder et al., 2015) |
| *Urumqi (Winter) | | | | | | (46%) | (54%) | | |
| *Xining (Winter) | | | | | | (51%) | (49%) | | (Zhong et al., 2023) |
| *Lanzhou (Winter) | | | | | | (60%) | (40%) | | |
| *Yinchuan (Winter) | | | | | | (30%) | (70%) | | |
| *Xian (Winter) | (19%) | (12%) | (13%) | | | | OOA (28%) | (28%) | (Lei et al., 2019) |
| *Xian (Summer) | | (7%) | (1%) | | | | OOA (75%) | (17%) | |
| *Yangzhou (Autumn to early Spring) | (24%) | (19%) | | | | | (47%) | | (Chen et al., 2020) |

| | | | |
|---|---|---|---|
| *Nanjing (Spring) | (58%) | (42%) | (Bao et al., 2022) |
| *Nanjing (Summer) | (44%) | (56%) | |
| *Nanjing (Autumn) | (75%) | (25%) | |
| *Nanjing (Winter) | (60%) | (40%) | |

***Note:***

**Nanjing SOA = anthropogenic SOA+ biogenic SOA + secondary nitrate and sulfate formation*

**Urumqi Xining Lanzhou Yinchuan SOA = HO–OOA1 + HO–OOA2 + LO–OOA*

*Mexico SOA = LO–OOA+MO–OOA*

**Yangzhou SOA = LO–OOA+MO–OOA*

*Paris BBOA = LO–BBOA+MO–BBOA*

*Manaus BBOA = LO–BBOA+MO–BBOA*

*Manaus SOA = MO–OOA+LO–OOA+IEPOX–SOA*

*Athens SOA = SV–OOA+LV–OOA*

*Singapore HOA = HOA+O–HOA*

*Beijing CCOA = FFOA*

*Beijing (winter 2016)–SOA = aqOOA + OPOA+OOA*

*Beijing (winter 2020)–SOA = LO–OOA+MO–OOA*

$Xian_{lockdown}$ SOA = LO–OOA + MO–OOA

**Table S7.** The literature summary of MAC ($m^2\ g^{-1}$) from different BrC sources, which was obtained by the PMF–MLR method in different environments. All the results were categorized based on the locations of their observation sites (urban China, Qinghai–Tibet Plateau (QTP region), and other countries).

| Sites | BBOA | HOA | CCOA | LO–OOA | MO–OOA | References |
|---|---|---|---|---|---|---|
| **Urban China** | | | | | | |
| Xianghe (winter) | 3.40±0.16 | 0.50±0.16 | 5.73±0.32 | | | (Wang et al., 2019) |
| Guangzhou (Winter 2014) | 3.40±0.41 | 0.61±0.05 | | | 1.04±0.08 | (Qin et al., 2018) |
| $Xian_{normal}$ (winter) | 1.66±0.08 | 1.44±0.08 | 5.35±0.13 | 0.71±0.05 | –0.26±0.08 | (Zhang et al., 2022) |
| $Xian_{lockdown}$ (winter) | 2.39±0.13 | 1.92±0.19 | 5.22±0.19 | 2.08±0.14 | 0.73±0.14 | |
| Guangzhou (Summer; **This study**) | 1.91±0.21 | 2.57±0.28 | | | | |
| **QTP region** | | | | | | |
| Gaomeigu (Spring) | 2.78±0.39 | | | | 1.43±0.23 | (Tian et al., 2023) |
| QOMS (Spring) | 2.29±0.02 | | | | 0.60±0.03 | (Zhang et al., 2021b) |
| YBJ (Summer; **This study**) | 1.11–2.54 | 2.08±0.30 | | 0.15±0.08 | 0.18±0.08 | |
| **Other countries** | | | | | | |
| Delhi (winter) | 0.86 | 0.42 | | 0.67 | | (Singh et al., 2021) |
| Manaus (Summer+Autumn) | (LO–BBOA) 1.5±0.07<br>(MO–BBOA) 0.82±0.01 | 2.04±0.14 | | 0.01±0.02 | 0.01±0.02 | (De Sá et al., 2019) |
| Athens (winter) | 7.63±0.74 | 1.34±0.49 | | 4.02±0.44 | 1.98±0.33 | (Kaskaoutis et al., 2021) |
| Paris (winter) | (LOBBOA) 4.86±0.18<br>(MO–BBOA) 2.02 ±0.12 | 1.06±0.23 | | (OOA) 0.55±0.05 | | (Zhang et al., 2020c) |
| Central Alabama (Summer) | 1.35±0.06 | | | 0.03±0.02 | –0.01±0.01 | (Washenfelder et al., 2015) |
| Mexico (Spring) | 1.82±0.02 | 1.76±0.03 | | 0.01±0.04 | 0±0.01 | (Retama et al., 2022) |
| Mexico (Summer) | 0.4±0.14 | 1.47±0.07 | | 0.03±0.06 | 0.04±0.03 | |
| Mexico (winter) | 0.83±0.09 | 1.79±0.03 | | 0.97±0.06 | –0.14±0.02 | |
| Mexico (Winter to summer) | 1.73±0.02 | 1.75±0.02 | | 0.29±0.03 | 0±0.01 | |
| Singapore (winter) | | 0.97±0.33 | | 0.67±0.23 | | (Kasthuriarachchi et al., 2020) |

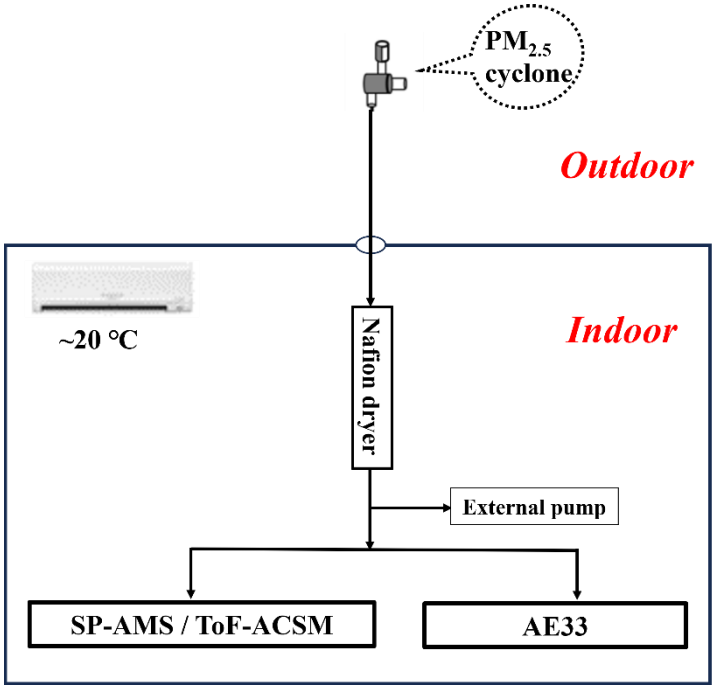


**Figure S1.** The setup diagram of instruments during campaign in Yangbajing and Guangzhou.

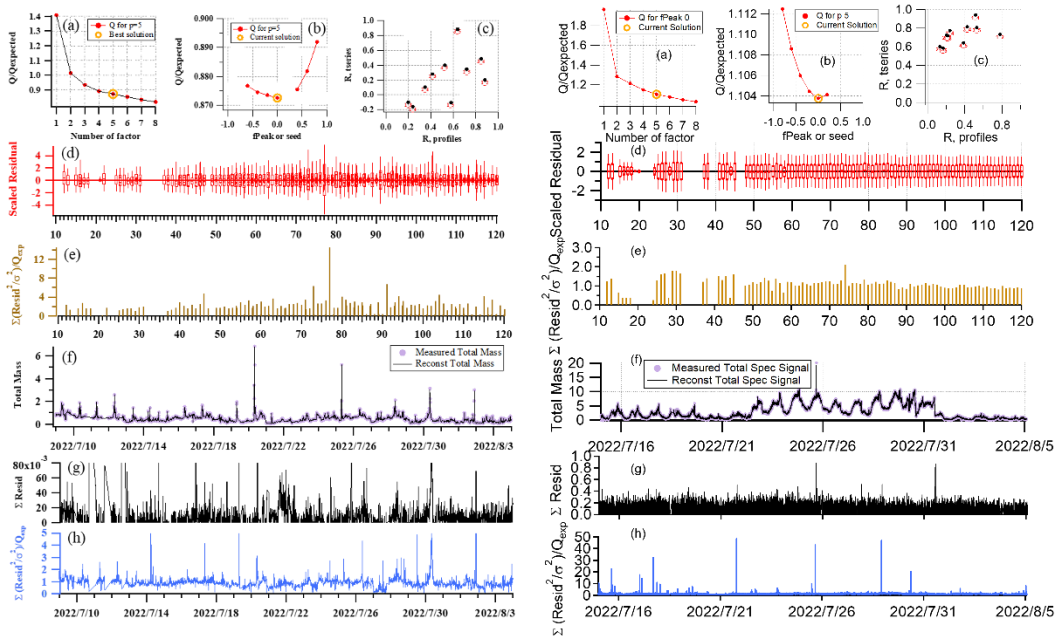


**Figure S2.** Diagnostics plots of factor selections in the unconstrained PMF at the YBJ site (left) and the GIG site (right).

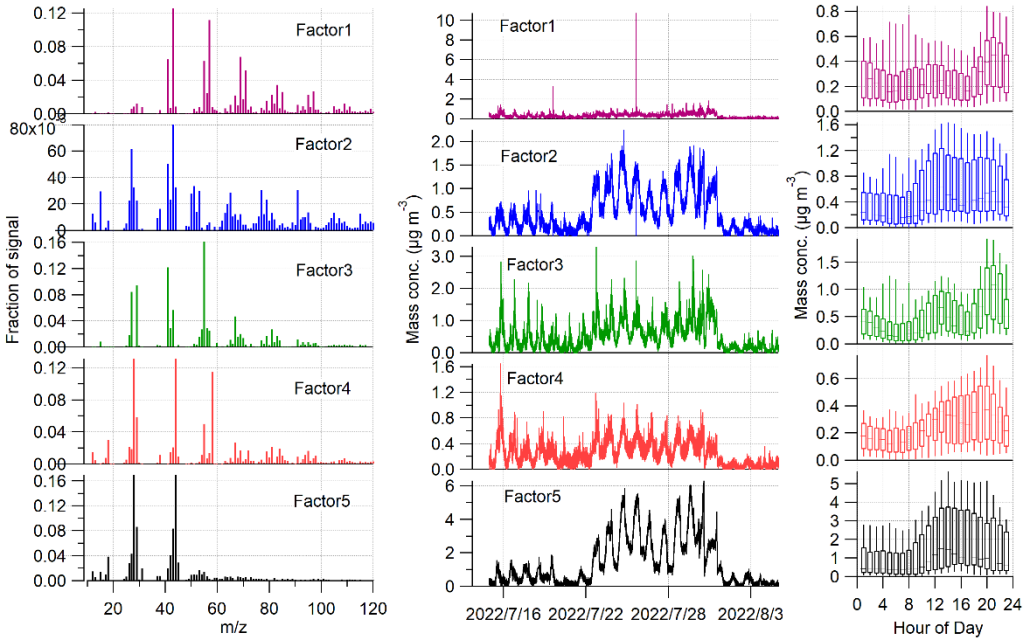


**Figure S3.** The 5–factor solution for OA sources in the unconstrained PMF at the GIG site.

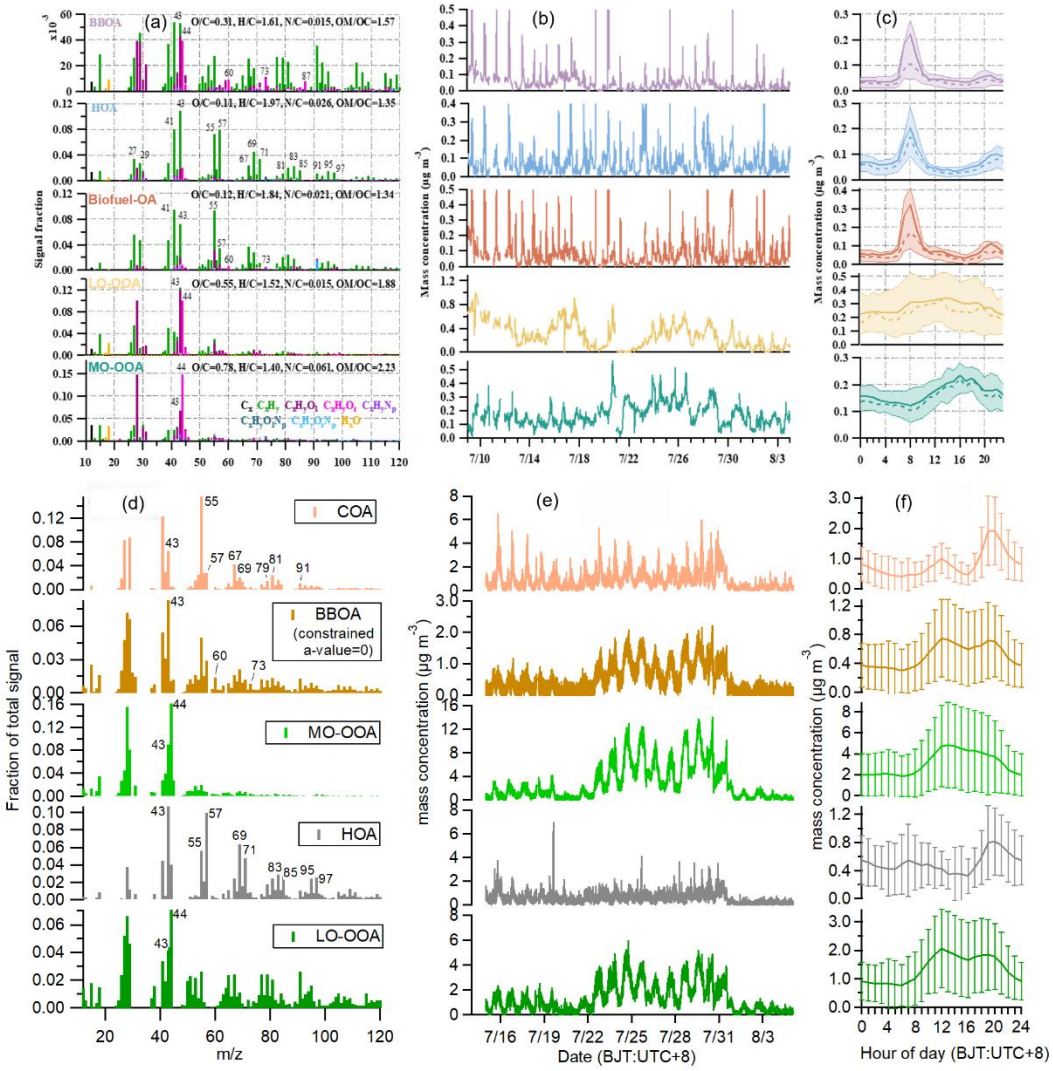


**Figure S4.** The final optimum solution for OA sources at the YBJ site and the GIG site.

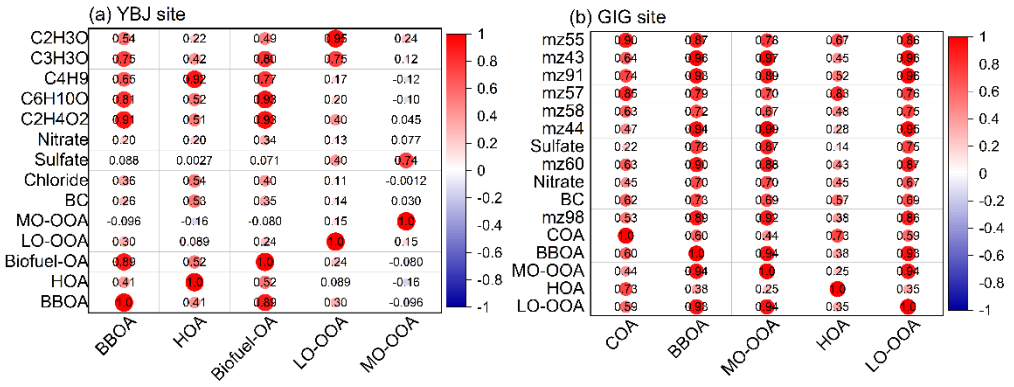


**Figure S5.** The Pearson's correlation coefficient (R) between the OA factor and tracers at the YBJ site and the GIG site.

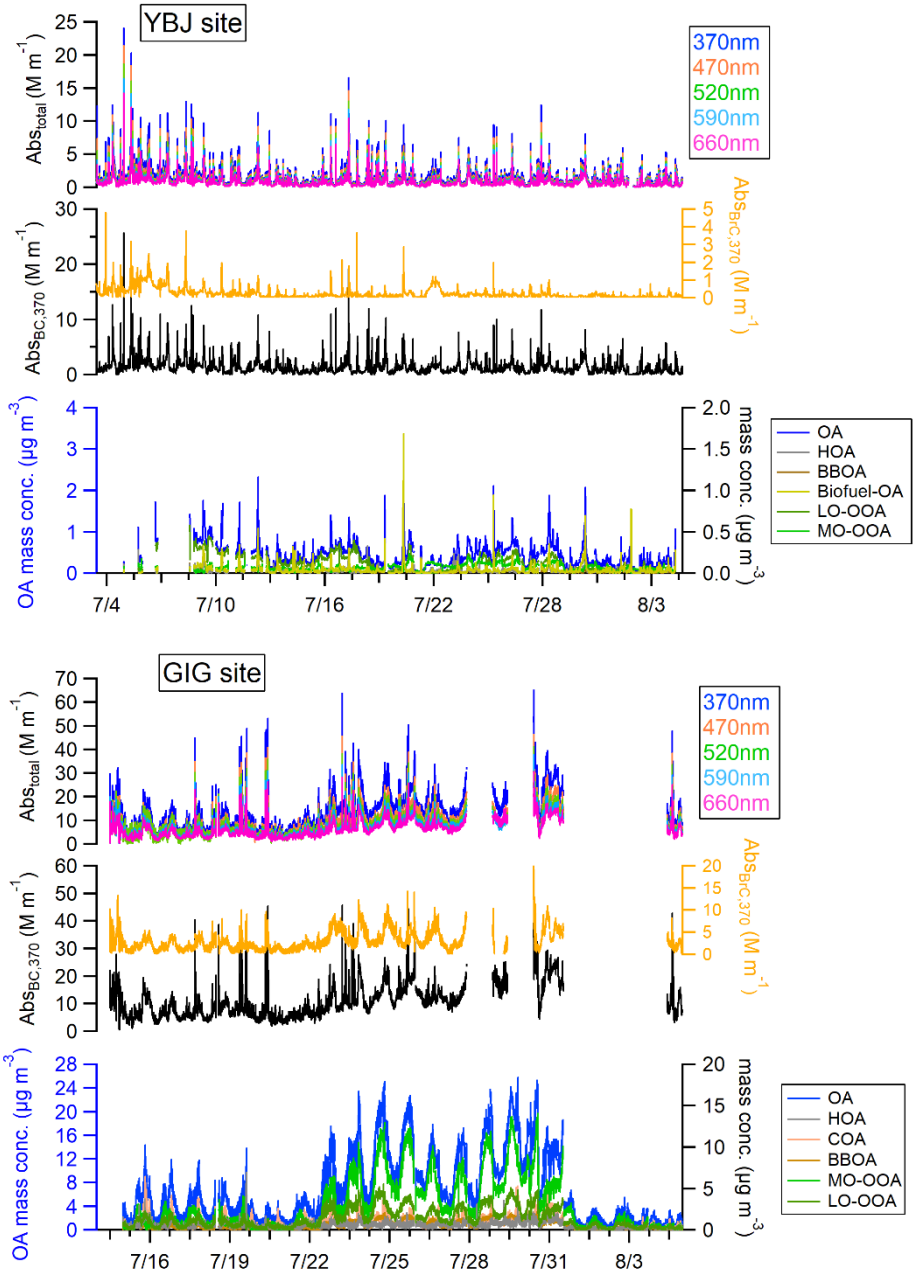


**Figure S6.** The time series of OA mass concentration and BrC light absorption coefficients at 370, 470, 520, 590, and 660 nm at the YBJ site and GIG site.

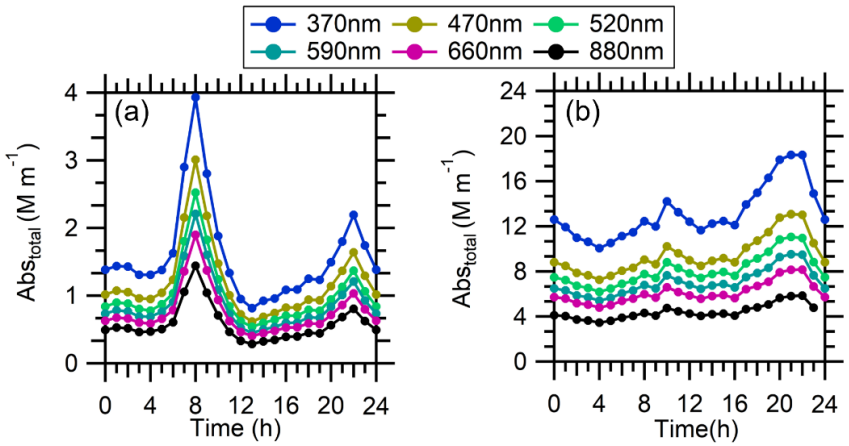


**Figure S7.** Diurnal variations of light absorption of total aerosol at seven wavelengths at the YBJ site (a) and the GIG site (b).

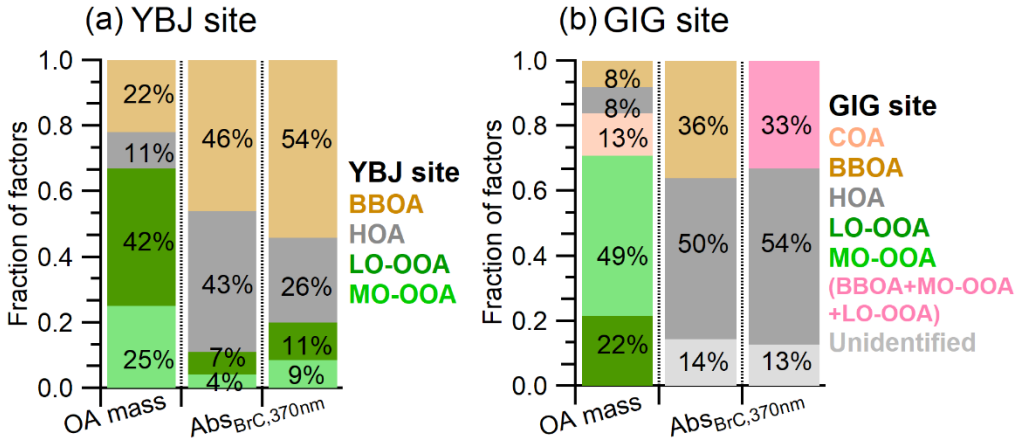


**Figure S8.** (a) The contributions of different OA factors to total OA (left) and contributions of different OA factors to BrC light absorption at 370 nm (Center and right; represent a upper and lower bound based on the different cases discussed in Section 2.5.1 and Text S2) at YBJ site (a) and GIG site (b).

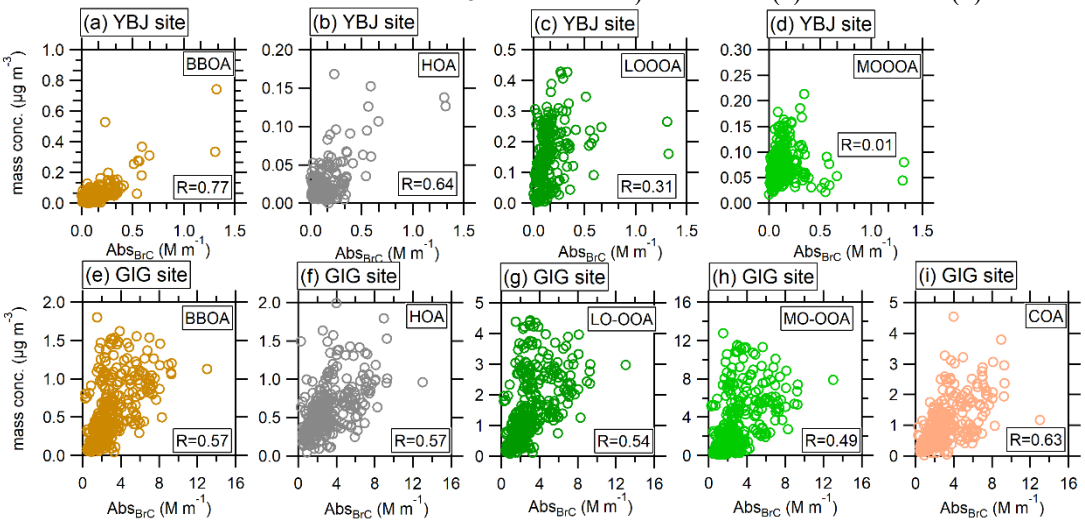


**Figure 9.** Scatter plots of brown carbon absorption at 370 nm versus the mass concentrations of OA factors during the campaign.

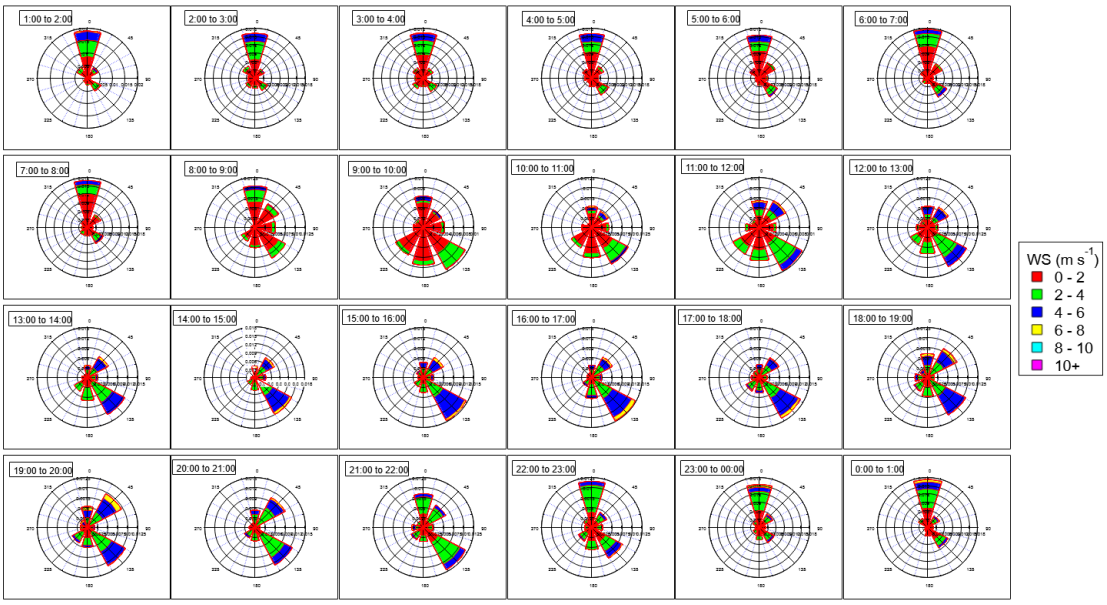


**Figure S10.** Hourly rose plots at the YBJ site.

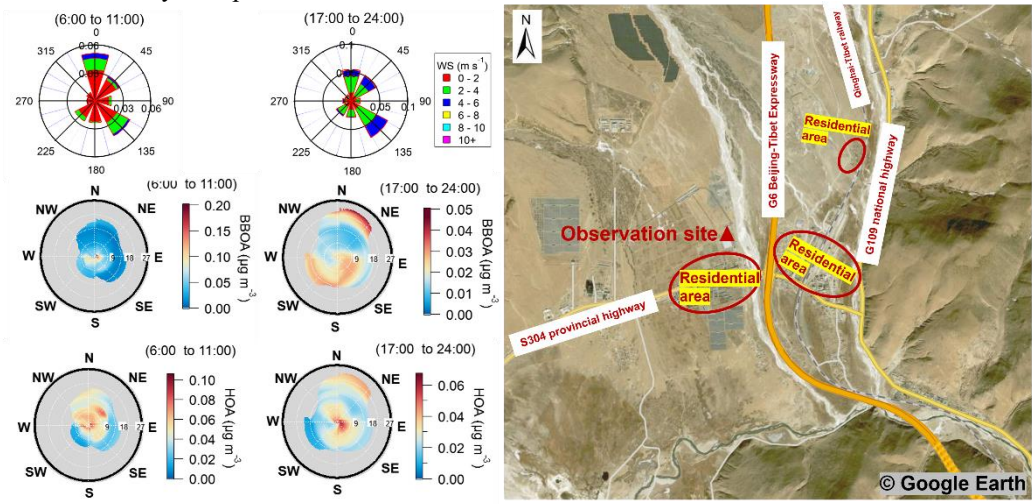


**Figure S11.** Rose plots and Bivariate polar plots of HOA and BBOA during morning peak (6:00 to 11:00) and evening peak (17:00 to 24:00). The unit of wind speed is km $h^{-1}$ in the Bivariate polar plots.

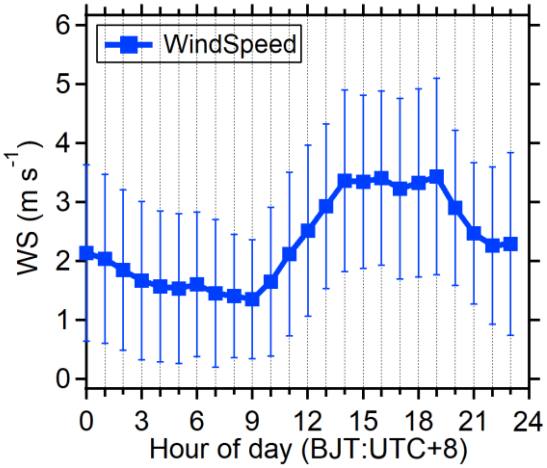


**Figure S12.** The diurnal variations of wind speed at the YBJ site

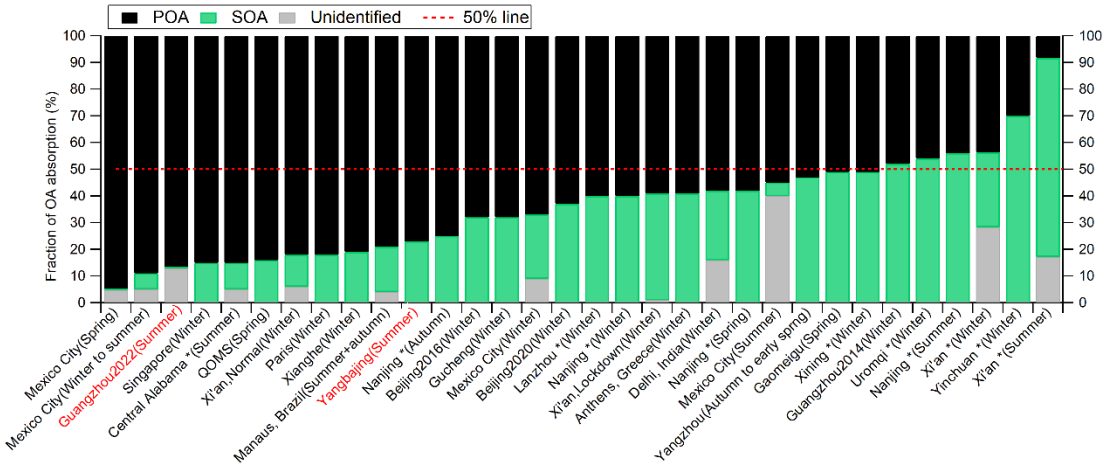


**Figure S13.** The summary of the contribution of organic aerosols from different sources to BrC absorption at 370 nm using the PMF–MLR method. The asterisks (*) represent the absorption contributions of soluble BrC from different sources at 365nm. The sources include POA (primary OA) and SOA (secondary OA). The dashed line represents 50% of BrC absorption.

**Reference**


Aiken, A. C., Salcedo, D., Cubison, M. J., Huffman, J. A., DeCarlo, P. F., Ulbrich, I. M., Docherty, K. S., Sueper, D., Kimmel, J. R., Worsnop, D. R., Trimborn, A., Northway, M., Stone, E. A., Schauer, J. J., Volkamer, R. M., Fortner, E., de Foy, B., Wang, J., Laskin, A., Shutthanandan, V., Zheng, J., Zhang, R., Gaffney, J., Marley, N. A., Paredes-Miranda, G., Arnott, W. P., Molina, L. T., Sosa, G., and Jimenez, J. L.: Mexico City aerosol analysis during MILAGRO using high resolution aerosol mass spectrometry at the urban supersite (T0) – Part 1: Fine particle composition and organic source apportionment, Atmos. Chem. Phys., 9, 6633-6653, 10.5194/acp-9-6633-2009, 2009.

Alfarra, M. R., Prevot, A. S. H., Szidat, S., Sandradewi, J., Weimer, S., Lanz, V. A., Schreiber, D., Mohr, M., and Baltensperger, U.: Identification of the Mass Spectral Signature of Organic Aerosols from Wood Burning Emissions, Environmental Science & Technology, 41, 5770-5777, 10.1021/es062289b, 2007.

Bao, M., Zhang, Y.-L., Cao, F., Lin, Y.-C., Hong, Y., Fan, M., Zhang, Y., Yang, X., and Xie, F.: Light absorption and source apportionment of water soluble humic-like substances (HULIS) in PM2.5 at Nanjing, China, Environmental Research, 206, 10.1016/j.envres.2021.112554, 2022.

Barrett, T. E. and Sheesley, R. J.: Year-round optical properties and source characterization of Arctic organic carbon aerosols on the North Slope, Alaska, Journal of Geophysical Research: Atmospheres, 122, 9319-9331, 10.1002/2016jd026194, 2017.

Cai, Y., Ye, C., Chen, W., Hu, W., Song, W., Peng, Y., Huang, S., Qi, J., Wang, S., Wang, C., Wu, C., Wang, Z., Wang, B., Huang, X., He, L., Gligorovski, S., Yuan, B., Shao, M., and Wang, X.: The important contribution of secondary formation and biomass burning to oxidized organic nitrogen (OON) in a polluted urban area: insights from in situ measurements of a chemical ionization mass spectrometer (CIMS), Atmospheric Chemistry and Physics, 23, 8855-8877, 10.5194/acp-23-8855-2023, 2023.

Canonaco, F., Crippa, M., Slowik, J. G., Baltensperger, U., and Prévôt, A. S. H.: SoFi, an IGOR-based interface for the efficient use of the generalized multilinear engine (ME-2) for the source apportionment: ME-2 application to aerosol mass spectrometer data, Atmospheric Measurement Techniques, 6, 3649-3661, 10.5194/amt-6-3649-2013, 2013.

Chen, Y., Xie, X., Shi, Z., Li, Y., Gai, X., Wang, J., Li, H., Wu, Y., Zhao, X., Chen, M., and Ge, X.: Brown carbon in atmospheric fine particles in Yangzhou, China: Light absorption properties and source apportionment, Atmospheric Research, 244, 10.1016/j.atmosres.2020.105028, 2020.

Crippa, M., Decarlo, P. F., Slowik, J. G., Mohr, C., Heringa, M. F., Chirico, R., Poulain, L., Freutel, F., Sciare, J., Cozic, J., Di Marco, C. F., Elsasser, M., Nicolas, J. B., Marchand, N., Abidi, E., Wiedensohler, A., Drewnick, F., Schneider, J., Borrmann, S., Nemitz, E., Zimmermann, R., Jaffrezo, J. L., Prévôt, A. S. H., and Baltensperger, U.: Wintertime aerosol chemical composition and source apportionment of the organic fraction in the metropolitan area of Paris, Atmospheric Chemistry and Physics, 13, 961-981, 10.5194/acp-13-961-2013, 2013.

Cui, Y. Y., Liu, S., Bai, Z., Bian, J., Li, D., Fan, K., McKeen, S. A., Watts, L. A., Ciciora, S. J., and Gao, R.-S.: Religious burning as a potential major source of atmospheric fine aerosols in summertime Lhasa on the Tibetan Plateau, Atmospheric Environment, 181, 186-191, 10.1016/j.atmosenv.2018.03.025, 2018.

De Sá, S. S., Rizzo, L. V., Palm, B. B., Campuzano-Jost, P., Day, D. A., Yee, L. D., Wernis, R., Isaacman-VanWertz, G., Brito, J., Carbone, S., Liu, Y. J., Sedlacek, A., Springston, S., Goldstein, A. H., Barbosa, H. M. J., Alexander, M. L., Artaxo, P., Jimenez, J. L., and Martin, S. T.: Contributions of biomass-burning, urban, and biogenic emissions to the concentrations and light-absorbing properties of particulate matter in central Amazonia during the dry season, Atmos. Chem. Phys., 19, 7973-8001, 10.5194/acp-19-7973-2019, 2019.

DeCarlo, P. F., Dunlea, E. J., Kimmel, J. R., Aiken, A. C., Sueper, D., Crounse, J., Wennberg, P. O., Emmons, L., Shinozuka, Y., Clarke, A., Zhou, J., Tomlinson, J., Collins, D. R., Knapp, D., Weinheimer, A. J., Montzka, D. D., Campos, T., and Jimenez, J. L.: Fast airborne aerosol size and chemistry measurements above Mexico City and Central Mexico during the MILAGRO campaign, Atmos. Chem. Phys., 8, 4027-4048, 10.5194/acp-8-4027-2008, 2008.

Du, W., Sun, Y. L., Xu, Y. S., Jiang, Q., Wang, Q. Q., Yang, W., Wang, F., Bai, Z. P., Zhao, X. D., and Yang, Y. C.: Chemical characterization of submicron aerosol and particle growth events at a national background site (3295 m a.s.l.) on the Tibetan Plateau, Atmospheric Chemistry and Physics, 15, 10811-10824, 10.5194/acp-15-10811-2015, 2015.

Duan, J., Huang, R. J., Gu, Y., Lin, C., Zhong, H., Xu, W., Liu, Q., You, Y., Ovadnevaite, J., Ceburnis, D., Hoffmann, T., and O'Dowd, C.: Measurement report: Large contribution of biomass burning and aqueous-phase processes to the wintertime secondary organic aerosol formation in Xi'an, Northwest China, Atmos. Chem. Phys., 22, 10139-10153, 10.5194/acp-22-10139-2022, 2022.

Florou, K., Papanastasiou, D. K., Pikridas, M., Kaltsonoudis, C., Louvaris, E., Gkatzelis, G. I., Patoulias, D., Mihalopoulos, N., and Pandis, S. N.: The contribution of wood burning and other pollution sources to wintertime organic aerosol levels in two Greek cities, Atmospheric Chemistry and Physics, 17, 3145-3163, 10.5194/acp-17-3145-2017, 2017.

Hu, W., Hu, M., Hu, W., Jimenez, J. L., Yuan, B., Chen, W., Wang, M., Wu, Y., Chen, C., Wang, Z., Peng, J., Zeng, L., and Shao, M.: Chemical composition, sources, and aging process of submicron aerosols in Beijing: Contrast between summer and winter, Journal of Geophysical Research: Atmospheres, 121, 1955-1977, 10.1002/2015jd024020, 2016.

Hu, W. W., Hu, M., Yuan, B., Jimenez, J. L., Tang, Q., Peng, J. F., Hu, W., Shao, M., Wang, M., Zeng, L. M., Wu, Y. S., Gong, Z. H., Huang, X. F., and He, L. Y.: Insights on organic aerosol aging and the influence of coal combustion at a regional receptor site of central eastern China, Atmospheric Chemistry and Physics, 13, 10095-10112, 10.5194/acp-13-10095-2013, 2013.

Huang, R.-J., Wang, Y., Cao, J., Lin, C., Duan, J., Chen, Q., Li, Y., Gu, Y., Yan, J., Xu, W., Fröhlich, R., Canonaco, F., Bozzetti, C., Ovadnevaite, J., Ceburnis, D., Canagaratna, M. R., Jayne, J., Worsnop, D. R., El-Haddad, I., Prévôt, A. S. H., and O'Dowd, C. D.: Primary emissions versus secondary formation of fine particulate matter in the most polluted city (Shijiazhuang) in North China, Atmospheric Chemistry and Physics, 19, 2283-2298, 10.5194/acp-19-2283-2019, 2019.

Kaskaoutis, D. G., Grivas, G., Stavroulas, I., Bougiatioti, A., Liakakou, E., Dumka, U. C., Gerasopoulos, E., and Mihalopoulos, N.: Apportionment of black and brown carbon spectral absorption sources in the urban environment of Athens, Greece, during winter, Science of The Total Environment, 801, 10.1016/j.scitotenv.2021.149739, 2021.

Kasthuriarachchi, N. Y., Rivellini, L. H., Adam, M. G., and Lee, A. K. Y.: Light Absorbing Properties of Primary and Secondary Brown Carbon in a Tropical Urban Environment, Environ Sci Technol, 54, 10808-10819, 10.1021/acs.est.0c02414, 2020.

Lanz, V. A., Alfarra, M. R., Baltensperger, U., Buchmann, B., Hueglin, C., and Prévôt, A. S. H.: Source apportionment of submicron organic aerosols at an urban site by factor analytical modelling of aerosol mass spectra, Atmospheric Chemistry and Physics, 7, 1503-1522, 10.5194/acp-7-1503-2007, 2007.

Lei, Y., Shen, Z., Zhang, T., Lu, D., Zeng, Y., Zhang, Q., Xu, H., Bei, N., Wang, X., and Cao, J.: High time resolution observation of PM2.5 Brown carbon over Xi'an in northwestern China: Seasonal variation and source apportionment, Chemosphere, 237, 10.1016/j.chemosphere.2019.124530, 2019.

Ng, N. L., Canagaratna, M. R., Jimenez, J. L., Chhabra, P. S., Seinfeld, J. H., and Worsnop, D. R.: Changes in organic aerosol composition with aging inferred from aerosol mass spectra, Atmospheric Chemistry and Physics, 11, 6465-6474, 10.5194/acp-11-6465-2011, 2011a.

Ng, N. L., Canagaratna, M. R., Jimenez, J. L., Zhang, Q., Ulbrich, I. M., and Worsnop, D. R.: Real-Time Methods for Estimating Organic Component Mass Concentrations from Aerosol Mass Spectrometer Data, Environmental Science & Technology, 45, 910-916, 10.1021/es102951k, 2011b.

Qin, Y. M., Tan, H. B., Li, Y. J., Li, Z. J., Schurman, M. I., Liu, L., Wu, C., and Chan, C. K.: Chemical characteristics of brown carbon in atmospheric particles at a suburban site near Guangzhou, China, Atmospheric Chemistry and Physics, 18, 16409-16418, 10.5194/acp-18-16409-2018, 2018.

Retama, A., Ramos-Cerón, M., Rivera-Hernández, O., Allen, G., and Velasco, E.: Aerosol optical properties and brown carbon in Mexico City, Environmental Science: Atmospheres, 2, 315-334, 10.1039/d2ea00006g, 2022.

Singh, A., Rastogi, N., Kumar, V., Slowik, J. G., Satish, R., Lalchandani, V., Thamban, N. M., Rai, P., Bhattu, D., Vats, P., Ganguly, D., Tripathi, S. N., and Prévôt, A. S. H.: Sources and characteristics of light-absorbing fine particulates over Delhi through the synergy of real-time optical and chemical measurements, ATMOSPHERIC ENVIRONMENT, 252, 10.1016/j.atmosenv.2021.118338, 2021.

Sun, J., Zhang, Q., Canagaratna, M. R., Zhang, Y., Ng, N. L., Sun, Y., Jayne, J. T., Zhang, X., Zhang, X., and Worsnop, D. R.: Highly time- and size-resolved characterization of submicron aerosol particles in Beijing using an Aerodyne Aerosol Mass Spectrometer, Atmospheric Environment, 44, 131-140, 10.1016/j.atmosenv.2009.03.020, 2010.

Sun, J., Xie, C., Xu, W., Chen, C., Ma, N., Xu, W., Lei, L., Li, Z., He, Y., Qiu, Y., Wang, Q., Pan, X., Su, H., Cheng, Y., Wu, C., Fu, P., Wang, Z., and Sun, Y.: Light absorption of black carbon and brown carbon in winter in North China Plain: comparisons between urban and rural sites, Science of The Total Environment, 770, 10.1016/j.scitotenv.2020.144821, 2021.

Tian, J., Wang, Q., Ma, Y., Wang, J., Han, Y., and Cao, J.: Impacts of biomass burning and photochemical processing on the light absorption of brown carbon in the southeastern Tibetan Plateau, Atmospheric Chemistry and Physics, 23, 1879-1892, 10.5194/acp-23-1879-2023, 2023.

Tian, J., Wang, Q., Zhang, Y., Yan, M., Liu, H., Zhang, N., Ran, W., and Cao, J.: Impacts of primary

emissions and secondary aerosol formation on air pollution in an urban area of China during the COVID-19 lockdown, Environ Int, 150, 106426, 10.1016/j.envint.2021.106426, 2021.
Ulbrich, I. M., Canagaratna, M. R., Zhang, Q., Worsnop, D. R., and Jimenez, J. L.: Interpretation of organic components from Positive Matrix Factorization of aerosol mass spectrometric data, Atmospheric Chemistry and Physics, 9, 2891-2918, 10.5194/acp-9-2891-2009, 2009.
Wang, J., Nie, W., Cheng, Y., Shen, Y., Chi, X., Wang, J., Huang, X., Xie, Y., Sun, P., Xu, Z., Qi, X., Su, H., and Ding, A.: Light absorption of brown carbon in eastern China based on 3-year multi-wavelength aerosol optical property observations and an improved absorption Ångström exponent segregation method, Atmospheric Chemistry and Physics, 18, 9061-9074, 10.5194/acp-18-9061-2018, 2018.
Wang, Q., Ye, J., Wang, Y., Zhang, T., Ran, W., Wu, Y., Tian, J., Li, L., Zhou, Y., Hang Ho, S. S., Dang, B., Zhang, Q., Zhang, R., Chen, Y., Zhu, C., and Cao, J.: Wintertime Optical Properties of Primary and Secondary Brown Carbon at a Regional Site in the North China Plain, Environmental Science & Technology, 53, 12389-12397, 10.1021/acs.est.9b03406, 2019.
Wang, X., Chakrabarty, R. K., Schwarz, J. P., Murphy, S. M., Levin, E. J. T., Howell, S. G., Guo, H., Campuzano-Jost, P., and Jimenez, J. L.: Dark brown carbon from biomass burning contributes to significant global-scale positive forcing, One Earth, 10.1016/j.oneear.2025.101205, 2025.
Wang, Y. C., Huang, R. J., Ni, H. Y., Chen, Y., Wang, Q. Y., Li, G. H., Tie, X. X., Shen, Z. X., Huang, Y., Liu, S. X., Dong, W. M., Xue, P., Fröhlich, R., Canonaco, F., Elser, M., Daellenbach, K. R., Bozzetti, C., El Haddad, I., Prévôt, A. S. H., Canagaratna, M. R., Worsnop, D. R., and Cao, J. J.: Chemical composition, sources and secondary processes of aerosols in Baoji city of northwest China, Atmospheric Environment, 158, 128-137, 10.1016/j.atmosenv.2017.03.026, 2017.
Washenfelder, R. A., Attwood, A. R., Brock, C. A., Guo, H., Xu, L., Weber, R. J., Ng, N. L., Allen, H. M., Ayres, B. R., Baumann, K., Cohen, R. C., Draper, D. C., Duffey, K. C., Edgerton, E., Fry, J. L., Hu, W. W., Jimenez, J. L., Palm, B. B., Romer, P., Stone, E. A., Wooldridge, P. J., and Brown, S. S.: Biomass burning dominates brown carbon absorption in the rural southeastern United States, Geophysical Research Letters, 42, 653-664, https://doi.org/10.1002/2014GL062444, 2015.
Xie, C., Xu, W., Wang, J., Wang, Q., Liu, D., Tang, G., Chen, P., Du, W., Zhao, J., Zhang, Y., Zhou, W., Han, T., Bian, Q., Li, J., Fu, P., Wang, Z., Ge, X., Allan, J., Coe, H., and Sun, Y.: Vertical characterization of aerosol optical properties and brown carbon in winter in urban Beijing, China, Atmospheric Chemistry and Physics, 19, 165-179, 10.5194/acp-19-165-2019, 2019.
Xu, J., Zhang, Q., Chen, M., Ge, X., Ren, J., and Qin, D.: Chemical composition, sources, and processes of urban aerosols during summertime in northwest China: insights from high-resolution aerosol mass spectrometry, Atmospheric Chemistry and Physics, 14, 12593-12611, 10.5194/acp-14-12593-2014, 2014.
Xu, W., Sun, Y., Wang, Q., Zhao, J., Wang, J., Ge, X., Xie, C., Zhou, W., Du, W., Li, J., Fu, P., Wang, Z., Worsnop, D. R., and Coe, H.: Changes in Aerosol Chemistry From 2014 to 2016 in Winter in Beijing: Insights From High-Resolution Aerosol Mass Spectrometry, Journal of Geophysical Research: Atmospheres, 124, 1132-1147, 10.1029/2018jd029245, 2019.
Yue, S., Bikkina, S., Gao, M., Barrie, L. A., Kawamura, K., and Fu, P.: Sources and Radiative Absorption of Water-Soluble Brown Carbon in the High Arctic Atmosphere, Geophysical Research Letters, 46, 14881-14891, 10.1029/2019gl085318, 2019.
Yue, S., Zhu, J., Chen, S., Xie, Q., Li, W., Li, L., Ren, H., Su, S., Li, P., Ma, H., Fan, Y., Cheng, B., Wu, L., Deng, J., Hu, W., Ren, L., Wei, L., Zhao, W., Tian, Y., Pan, X., Sun, Y., Wang, Z., Wu, F., Liu, C.-Q., Su, H., Penner, J. E., Pöschl, U., Andreae, M. O., Cheng, Y., and Fu, P.: Brown carbon from biomass burning imposes strong circum-Arctic warming, One Earth, 5, 293-304, 10.1016/j.oneear.2022.02.006, 2022.
Zhang, Q., Worsnop, D. R., Canagaratna, M. R., and Jimenez, J. L.: Hydrocarbon-like and oxygenated organic aerosols in Pittsburgh: Insights into sources and processes of organic aerosols, Atmos. Chem. Phys., 5, 3289, 2005a.
Zhang, Q., Canagaratna, M. R., Jayne, J. T., Worsnop, D. R., and Jimenez, J. L.: Time and size-resolved chemical composition of submicron particles in Pittsburgh - Implications for aerosol sources and processes, J. Geophys. Res., 110, 10, 2005b.
Zhang, Q., Jimenez, J. L., Canagaratna, M. R., Ulbrich, I. M., Ng, N. L., Worsnop, D. R., and Sun, Y.: Understanding atmospheric organic aerosols via factor analysis of aerosol mass spectrometry: a review, Anal Bioanal Chem, 401, 3045-3067, 10.1007/s00216-011-5355-y, 2011.
Zhang, Q., Shen, Z., Zhang, L., Zeng, Y., Ning, Z., Zhang, T., Lei, Y., Wang, Q., Li, G., Sun, J., Westerdahl, D., Xu, H., and Cao, J.: Investigation of Primary and Secondary Particulate Brown Carbon in Two Chinese Cities of Xi'an and Hong Kong in Wintertime, Environmental Science & Technology, 54, 3803-3813, 10.1021/acs.est.9b05332, 2020a.

Zhang, Q., Shen, Z., Zhang, T., Kong, S., Lei, Y., Wang, Q., Tao, J., Zhang, R., Wei, P., Wei, C., Cui, S., Cheng, T., Ho, S. S. H., Li, Z., Xu, H., and Cao, J.: Spatial distribution and sources of winter black carbon and brown carbon in six Chinese megacities, Science of The Total Environment, 762, 143075, https://doi.org/10.1016/j.scitotenv.2020.143075, 2021a.

Zhang, X., Xu, J., and Kang, S.: Chemical characterization of submicron particulate matter (PM1) emitted by burning highland barley in the northeastern part of the Qinghai–Tibet Plateau, Atmospheric Environment, 224, 10.1016/j.atmosenv.2020.117351, 2020b.

Zhang, X., Xu, J., Kang, S., Zhang, Q., and Sun, J.: Chemical characterization and sources of submicron aerosols in the northeastern Qinghai–Tibet Plateau: insights from high-resolution mass spectrometry, Atmospheric Chemistry and Physics, 19, 7897-7911, 10.5194/acp-19-7897-2019, 2019.

Zhang, X., Xu, J., Kang, S., Sun, J., Shi, J., Gong, C., Sun, X., Du, H., Ge, X., and Zhang, Q.: Regional Differences in the Light Absorption Properties of Fine Particulate Matter Over the Tibetan Plateau: Insights From HR-ToF-AMS and Aethalometer Measurements, Journal of Geophysical Research: Atmospheres, 126, 10.1029/2021jd035562, 2021b.

Zhang, Y., Wang, Q., Tian, J., Li, Y., Liu, H., Ran, W., Han, Y., Prévôt, A. S. H., and Cao, J.: Impact of COVID-19 lockdown on the optical properties and radiative effects of urban brown carbon aerosol, Geoscience Frontiers, 13, 101320, https://doi.org/10.1016/j.gsf.2021.101320, 2022.

Zhang, Y., Albinet, A., Petit, J.-E., Jacob, V., Chevrier, F., Gille, G., Pontet, S., Chrétien, E., Dominik-Sègue, M., Levigoureux, G., Močnik, G., Gros, V., Jaffrezo, J.-L., and Favez, O.: Substantial brown carbon emissions from wintertime residential wood burning over France, Science of The Total Environment, 743, 10.1016/j.scitotenv.2020.140752, 2020c.

Zhong, M., Xu, J., Wang, H., Gao, L., Zhu, H., Zhai, L., Zhang, X., and Zhao, W.: Characterizing water-soluble brown carbon in fine particles in four typical cities in northwestern China during wintertime: integrating optical properties with chemical processes, Atmos. Chem. Phys., 23, 12609-12630, 10.5194/acp-23-12609-2023, 2023.

Zhu, C.-S., Cao, J.-J., Hu, T.-F., Shen, Z.-X., Tie, X.-X., Huang, H., Wang, Q.-Y., Huang, R.-J., Zhao, Z.-Z., Močnik, G., and Hansen, A. D. A.: Spectral dependence of aerosol light absorption at an urban and a remote site over the Tibetan Plateau, Science of The Total Environment, 590-591, 14-21, https://doi.org/10.1016/j.scitotenv.2017.03.057, 2017.

Zhu, C. S., Qu, Y., Huang, H., Chen, J., Dai, W. T., Huang, R. J., and Cao, J. J.: Black Carbon and Secondary Brown Carbon, the Dominant Light Absorption and Direct Radiative Forcing Contributors of the Atmospheric Aerosols Over the Tibetan Plateau, Geophysical Research Letters, 48, 10.1029/2021gl092524, 2021.